Title

Accurate perceptual decision driven by distinct population dynamics in association and sensory cortex

Authors/Affiliations

Yuma Osako*, Tomoya Ohnuki, Hiroyuki Manabe, Yoshio Sakurai, Junya Hirokawa*

Laboratory of Neural Information, Graduate School of Brain Science, Doshisha University, 1-3 Tatara Miyakodani, Kyotanabe, Kyoto, 610-0394, Japan.

Author List Footnotes

n/a

Contact Info

*Correspondence: yyosako@gmail.com (for Y.O.), jhirokaw@mail.doshisha.ac.jp (for J.H.)

Summary

During visual detection tasks, subjects sometimes fail to respond to identical visual stimuli even when the stimuli are registered on their retinas. It is widely assumed that variability in detection performance is attributed to the fidelity of the visual responses in visual cortical areas, which could be modulated by fluctuations of subjective internal states such as vigilance, attention, and reward experiences. However, it is not clear what neural ensembles represent such different internal states. Here, we utilized a behavioral task that differentiated distinct perceptual states to identical stimuli, and analyzed neuronal responses simultaneously recorded from both primary visual cortex (V1) and posterior parietal cortex (PPC) during the task. We found that population activity differed across choice types with the major contribution of non-sensory neurons, rather than visually-responsive neurons, in V1 as well as PPC. The distinct population-level activity in V1, but not PPC, was restricted within the stimulus presentation epoch, which was distinguished from pre-stimulus background activity and was supported by near-zero noise correlation. These results indicate a major contribution of non-sensory neurons in V1 for population-level computation that enables behavioral responses from visual information.

Introduction

Identical sensory stimuli sometimes evoke different perceptual and behavioral responses. For instance, in sensory detection task, human or animal subjects are instructed or well-trained to

reliably report the presence and absence of sensory stimuli to obtain rewards. When the sensory evidence is near threshold for the decision criterion, the subjects' reports vary across trials despite the best efforts of subjects to get rewards. Interestingly, even if they report the absence of stimuli, it is sometimes possible that they could correctly guess the contents of the stimuli above chance level if they are forced to answer[1–8]. Revealing the neural mechanisms underlying such trial-by-trial variability of perceptual reports is crucial to understand how the brain exploits sensory information for optimal decision making.

The trial-by-trial variance of the responses to identical stimuli is believed to reflect noises in conversion of sensory information into motor outputs[9]. It has been demonstrated that variability of firing rates of sensory neurons is responsible for the trial-by-trial variability of choices[10–14]. However, the accumulating evidence suggests that perceptual decision is also significantly affected by latent subjective states reflecting task engagement[15,16]. For instance, it is known that behavioral response variability is correlated with mind wondering in humans[17] and fluctuations of physiological and behavioral states in animals[18–22]. These drifts of subjective states could be partially attributed to fluctuation of cortical states[22–28], in which synchronization and desynchronization of many neurons in particular areas of cortex could affect efficiency of the population coding[29,30]. In addition, the task engagement is known to be modulated by trial-by-trial experience of decisions and its outcomes[31–37], which is supported by distinct populations of neurons in association areas [38,3940,41]. Furthermore, some studies suggest that neurons which are not explicitly responding to stimulus, contribute to the texture discriminations in somatosensory cortex[42], working memory coding in prefrontal cortex[43], stimulus/choice coding in auditory cortex[44] and category representation in prefrontal cortex[44]. These studies highlight the potential contribution of non-sensory neurons in modulating sensory processing resulting in trial-by-trial variability of responses. However, it has been elusive how non-sensory neurons are coordinated with sensory neurons for optimal sensory decisions.

Many previous studies revealed that neural activity in primary visual cortex (V1) and posterior parietal cortex (PPC) play a key role for visual detection behavior[45–47]. Patients with V1 lesion report subjective blindness[48,49] and direct optogenetic inhibition of rodent V1 impaired visual detection behavior[50]. On the other hand, electric stimulation of PPC generates artificial visual percepts in blind patients and healthy subjects[51–53], while such artificial percepts is highly correlated with V1 activity elicited by PPC stimulations. PPC also plays important roles in selective attention and reward-history bias[38,39] and regulates response properties of V1 neurons[54–56]. Recent imaging studies examined visual perceptual behavior during go/no-go detection task and found that visual responses in PPC is heavily modulated by task

requirements[57] and heterogenous recruitments of V1 neurons play an important role in visual detection[57,58]. Together, these studies support the notion that interactive activity between V1 and PPC forms distinct cortical states at population level that integrates task-relevant external signals[59–62] with internal states for subjective detection performance.

While imaging studies using head-fixed rodents are advantageous for recording many neurons across different cortical areas simultaneously, go/nogo task paradigm, which is often used in those experiments with head-fixed animals, is susceptible to subjective biases: go trials may contain false alarms and nogo trials may contain false rejections[63] due to fluctuating internal states as described above. To further classify such hidden behavioral states during the visual detection task, we previously developed a spatial-visual cue detection task for free-moving rats[2]. The task combines a two-alternative spatial choice task with a third option for void stimulus, which allowed us to differentiate three distinct visual detection states based on choice types during the task; hit trials (spontaneous correct choice), miss+ trials (missed responses but chose correct side when forced) and miss- trials (missed responses and chose the incorrect side when forced). By taking advantages of these relatively homogenous trials with distinct choice types to identical stimuli, we revealed distinct contributions of V1 and PPC neurons at population level for those choice types. In particular, these choice types are differentiated by distinct coordinated activities from non-sensory neurons rather than the fidelity of the visually-evoked activities in V1.

Results

Rats performed a visual detection task based on their internal threshold

We trained seven rats to perform a spatial visual-cue detection task (Fig.1a), which is essentially 3-alternative choice design and encourages animals to report the presence or the absence of the peripheral visual stimuli as described in our previous study[2]. Briefly, a trial was initiated by poking to the central port. Rats were rewarded by choosing peripheral ports in the trials where visual stimulus is presented (left or right) or by keeping nose in the central port in the trials where no stimulus is presented. In the half of the trials, the central port is closed 0.5 s after the stimulus presentation timing to force the animals to make the peripheral choices.

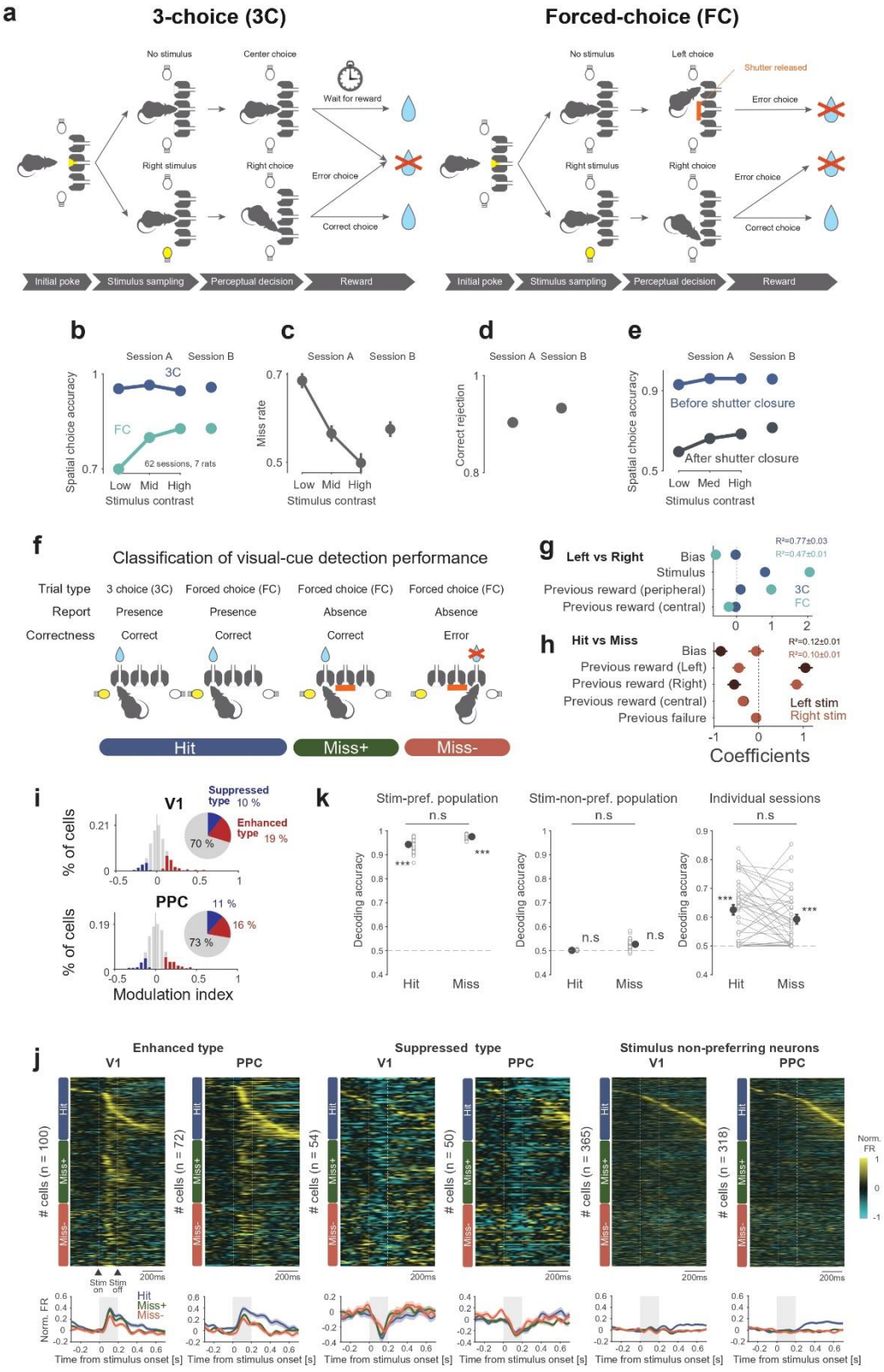
a
3-choice (3C)
Forced-choice (FC)
No stimulus
Center choice
Right stimulus
Right choice
Wait for reward
Error choice
Correct choice
Left choice
Shutter released
Initial poke
Stimulus sampling
Perceptual decision
Reward
b
Session A
Session B
3C
FC
62 sessions, 7 rats
Spatial choice accuracy
Low Mid High
Stimulus contrast
c
Miss rate
d
Correct rejection
e
Before shutter closure
After shutter closure
Low Med High
f
Classification of visual-cue detection performance
Trial type
Report
Correctness
3 choice (3C)
Forced choice (FC)
Presence
Absence
Correct
Error
Hit
Miss+
Miss-
g
Left vs Right
Bias
Stimulus
Previous reward (peripheral)
Previous reward (central)
R²=0.77±0.03
R²=0.47±0.01
h
Hit vs Miss
Previous reward (Left)
Previous reward (Right)
Previous reward (central)
Previous failure
R²=0.12±0.01
R²=0.10±0.01
Left stim
Right stim
Coefficients
i
V1
PPC
Suppressed type 10 %
Enhanced type 19 %
70 %
11 %
16 %
73 %
% of cells
Modulation index
k
Stim-pref. population
Stim-non-pref. population
Individual sessions
n.s
Decoding accuracy
Hit
Miss
j
Enhanced type
Suppressed type
Stimulus non-preferring neurons
cells (n = 100)
cells (n = 72)
cells (n = 54)
cells (n = 50)
cells (n = 365)
cells (n = 318)
Norm. FR
Stim on
Stim off
200ms
Time from stimulus onset [s]

Figure 1 | Neural recording in V1 and PPC during spatial visual-cue detection task. a, Schematics of behavioral paradigm. In 3C trials, central port was available, whereas it was shut when rats kept nose-poking in the central port more than 0.5s. **b**, Spatial choice accuracy in 3C and FC trials with graded visual contrast in session A and one contrast in session B. **c**, Miss rate in 3C trials. **d**, Correct rejection rate in 3C trials. **e**, Spatial choice accuracy before and after shutter closure in FC trials. **f**, Conceptual illustrating of three distinct choice types. We classified spontaneous correct response, forced correct response and forced error choice as Hit, Miss+ and Miss-, respectively. **g-h**, The impact of task parameters on behavioral variability using GLM fitting with several task parameters to Left/Right choice in 3C and FC (**g**), and to Hit/Miss choice in peripheral stimulus trials (**h**). **i**, Histogram of contralateral stimulus selectivity for V1 and PPC. Colors indicate neurons with significant selectivity (ROC, selectivity, permutation test, $P < 0.05$). Inset indicates proportion of neurons with significant selectivity. **j**, Trial-averaged neural activity for each choice type in Enhanced type stimulus preferring neurons, Suppressed type stimulus preferring neurons and stimulus non-preferring neurons in V1 and PPC. All responses were normalized by absolute peak subtracted mean response. Neurons sorted by max peak latency in hit trials. **k**, Decoding accuracies of contralateral stimulus presence for the stimulus preferring, non-preferring population and individual sessions.

To confirm whether rats have a steady internal detection criterion for visual detection, we alternated prove sessions with graded stimulus strength (session A) and neural recording sessions with a constant near-threshold stimulus strength (session B). In session A, as consistent with previous study, the peripheral choice accuracy in FC trials decreased from approximately 80% to 65% as the visual contrast decreased (Fig.1b, blue), while the accuracy was maintained at >90% regardless of visual contrast in the 3C trials (Fig. 1b, sky blue). The rats missed the visual stimuli more often (from 50% to 70%) as the visual contrast decreased (Fig.1c). They also showed >90% correct rejection performance when the visual stimulus was not actually emitted in 3C trials (Fig.1d). These results confirmed that the rats have a generalized strategy to make the peripheral choices only when their internal detection criterion is met. In addition, the rats showed the correct peripheral choices above chance level when the shutter forced them to make the peripheral choices after they chose to stay in the central port (Fig.1e, gray). These results suggest that the rats received visual information but did not exploit it maximumly. We labeled trials with the different choice types as Hit, Miss+, and Miss- according to the choice performances (Fig.1f). To find out the influence of trial history in those choice types, we conducted generalized linear model (GLM) analysis for the spatial choice (left and right) and hit/miss choice (Fig.1g-h). In FC trials, about half of the choice variance was explained by the model showing significant influences from previous peripheral rewards as well as the current stimulus direction. In contrast, in the 3C trials, the influence of rewards disappeared and the

77% of the choice variance was accounted by stimulus alone (Fig.1g). In addition, relatively small portion of the total variance (10%) for the Hit/Miss choices was explained with the model containing past rewards, in which major contribution was previous reward ipsilateral to the current stimulus (Fig.1h). These results suggest that our task successfully segregated trial-by-trial variability observed in detection tasks into distinct category (Hit, Miss+, Miss-) consisting of relatively homogeneous trials with minimum confounds of reward history bias.

Stimulus-preferring neurons in V1 and PPC were activated depending on choice types

We recorded neurons simultaneously from the right V1 (N_{V1} = 518 neurons) and PPC (N_{PPC} = 440 neurons) using chronic tetrode implants during the task performance (Extended Data Fig.3). To investigate effects of the choice types on visual responses of the neurons, we first identified stimulus preferring neurons by a ROC-based modulation index (see Methods). One third of the neurons showed significantly selective ($p < 0.05$, permutation test) for visual stimulus in V1 (29%, N = 154) and PPC (27%, N = 127) (Fig.1i).

Both V1 and PPC neurons showed stimulus-dependent activity (enhanced or suppressed from pre-stimulus baseline) regardless of the choice types (Fig.1j), even if the rats did not make the peripheral choices (Miss+ and Miss- trials). Decoding analysis of the stimulus (presence/absence) showed that the stimulus preferring population decoded stimulus presence near perfectly regardless of choice types, whereas the stimulus non-preferring population did not predict it (Fig.1k). The results confirmed that the activity during the stimulus epoch is evoked by visual stimulus but not by stimulus expectations. Though the decoding quality in individual sessions was varied due to the difference in number of the stimulus-preferring neurons recorded in each session, the mean decoding accuracy for the two choice types (0.61 ± 0.02 and 0.58 ± 0.02 for Hit and Miss, respectively) was significantly larger than chance ($p < 0.001$ and $p < 0.001$ for Hit and Miss, respectively, t-test) with no significant difference between the choice types ($p > 0.05$, x-test Fig.1k right). These results indicate that the missed responses are not sufficiently explained by the absence of visual information in visual cortex. Rather, all the choice types showed similar time course of mean firing rates in the stimulus-preferring neurons, particularly in V1, at least until the initial peak (~100 ms) of the stimulus responses

(Fig.1j). Time course of the stimulus non-preferring neurons in both V1 and PPC also did not

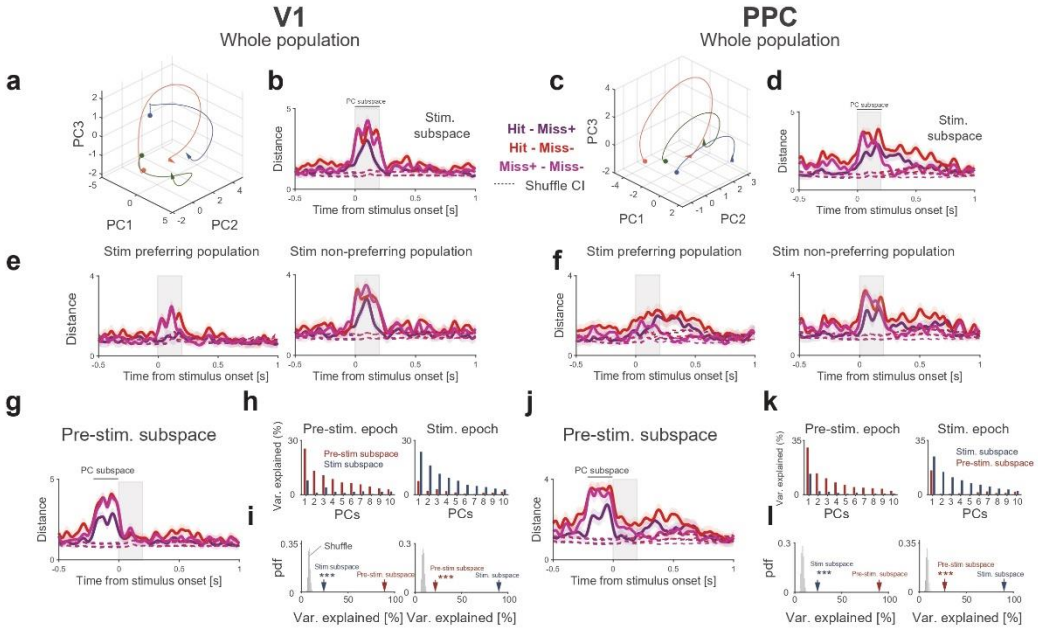

Figure 2 | Population dynamics in pre-stimulus and stimulus subspaces in V1 and PPC. a, c, Population responses of whole population projected onto three dimensions of the stimulus subspace from stimulus onset to stimulus offset (0-0.2s from stimulus onset) in V1 and PPC. Each color corresponds to choice types. **b, d**, Euclidian distance between pairs of conditions in PC subspace calculated from projections of **a**, **b**. Shaded area indicated stimulus presentation timing. Each plot was shown as Mean ± S.E and dashed line denotes 95% confidence interval of the shuffled distribution with 1000 shuffles. **e, f**, Same as in **c**, **d**, but calculated from the stimulus preferring and non-preferring population in V1 and PPC. **g, j**, Same as in **c**, **d**, but calculated from whole population which projected n-dimensions of the pre-stimulus subspaces (-0.2 – 0s from stimulus onset) in V1 and PPC. **h, k**, Percentages of stimulus subspace data variance (blue) and pre-stimulus data variance (red) for each epoch. **i, l**, Sum of variance explained from 10 PCs for each subspace. Histogram shows shuffled distributions with 1000 shuffles. Each significance marks were compared to shuffle data ($p < 0.001$, one-tailed test).

show clear differences on average among the choice types until 0.2 after the stimulus presentation (Fig.1j).

Significant contributions of non-sensory neurons in V1 as well as PPC for separating different choice types as population activity

We next address whether the choice types are separable at the level of the population activity. Principal component analysis (PCA) was applied to the stimulus epoch (0 – 0.2s after stimulus

onset) computing the weights of each neuron which is optimized to capture the variance of neural activity across the choice types. We identified three dimensions that captured 51, 50% for the whole population in V1 and PPC, respectively. As a result, the population dynamics showed unique trajectories associated with three different choice types (Fig.2a-b). To estimate the difference of neural trajectories, we computed Euclidian distance in the PC space between pairs of the choice types (see Methods). We found that the distance of all pairs peaked at the stimulus epoch as expected in both V1 and PPC (Fig.2c-d). Interestingly, whereas separations among all pairs of the choice types in V1 were mostly restricted within the epoch that built the subspace, the separations between Hit+ and the others spread beyond the corresponding epoch in PPC. To address the contributions of the different population types, we repeated the same analysis dividing the population into the stimulus preferring and non-preferring populations (capturing 63, 62% variance in the stimulus preferring population and 49, 48% variance in the stimulus non-preferring population in V1 and PPC, respectively). In stimulus preferring neuron population, separations of Hit-Miss+ were not evident in both V1 and PPC, whereas separations of Miss+-Miss- were well separated. These results suggest that similar quality of visual inputs is provided in Hit and Miss+ trials, at least in V1 level, whereas Miss- may not have sufficient quality of visual inputs. In contrast, the stimulus non-preferring population separated all choice types in both V1 and PPC (Fig.2f). To confirm the generality of the sustained activity, the same analysis was repeated in the pre-stimulus epoch. Separative population activity from the pre-stimulus subspace was sustained beyond the corresponding epoch in PPC(Fig.2j) but not in

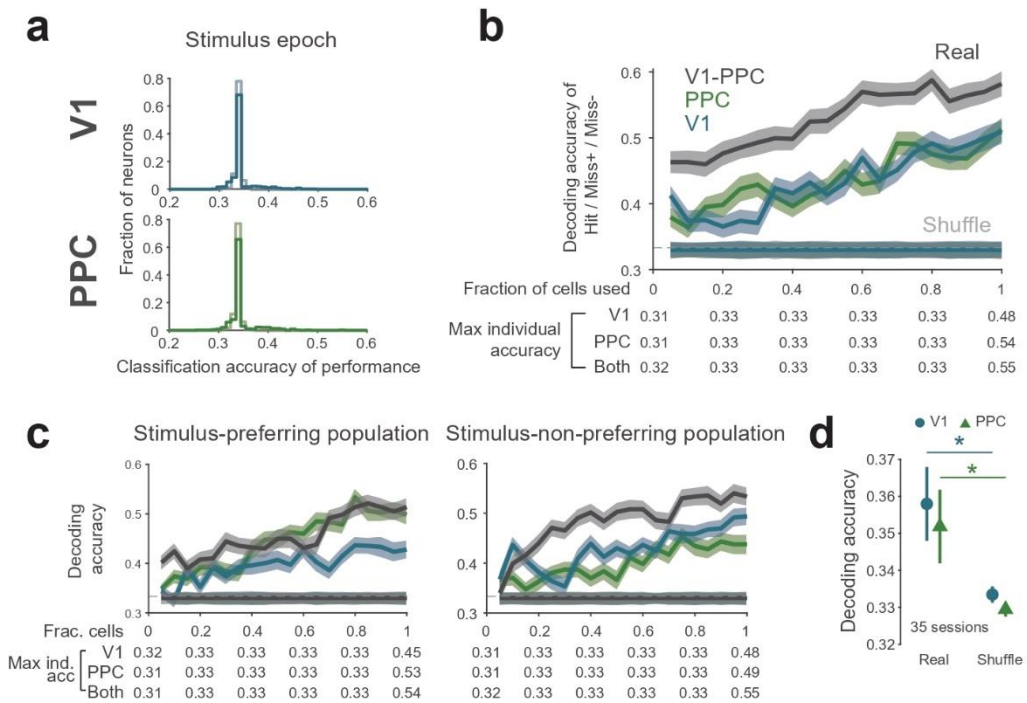

Figure 3 | Distributed representation by sequential population size. a, Histogram of decoding accuracy for choice types for individual neurons (colored line) and shuffled data (gray line) based on the normalized firing rate in stimulus presentation epoch (0-0.2s from stimulus onset) in V1 and PPC. **b**, Classification accuracy for choice types by sequential population size. Neurons we included by descending order based on histogram in **a** in whole population. Each line was shown as Mean ± 95% confidence interval. **c**, Same as in b, but only the stimulus preferring (left) and non-preferring neurons (right) were used. **d**, Classification accuracy for choice types in individual sessions (n = 35sessions). Real data showed significantly higher accuracy compared to shuffled data ($p < 0.05$, student t-test).

V1(Fig.2g) as consistent with the case in the stimulus epoch. Analysis of the variance in those different epochs suggests that neural subspace for one epoch (e.g., stimulus) captures only 30% of the variance in other epochs (e.g., pre-stimulus), suggesting dynamic change of neural states before and after the stimulus presentation. Together, these results emphasize the important role of the stimulus non-preferring neurons in V1 as a population activity for different choice types during stimulus presentation epoch, of which neural state is distinct from that in pre-stimulus epoch.

Population representation of choice types is distributed across heterogenous individual neurons

So far, we have addressed the distinct population activity across the choice types in the pre-stimulus and stimulus epochs. Given this finding, we asked whether the neural computation contributing to the choice types is only supported by individual neurons that contains the different choice type information, or neurons that have subtle information. We first used a multi-class linear support vector machine (SVM) algorithm to predict the choice types from the single neuron activities in the stimulus epoch (Fig.3a). Only a few neurons had a statistically significant decoding accuracy in both V1 and PPC (Fig.3a). This indicates that most of the single neurons does not have sufficient information to separate the choice types. We next addressed whether only subset of neurons with high selectivity to the choice types contributed to computation at the population level or the other neurons with low selectivity also contributed to population computation. We sorted the neurons based on the individual decoding accuracy in an ascending order, and gradually incorporated all the individual neurons. The classification accuracy increased in both V1 and PPC with incorporation of the neurons that had poor information of the choice types (Fig.3b). These results indicate that information of individual neurons for separating the choice types is poor but including these single neurons gradually improved separation of the choice types.

To confirm whether the non-sensory neurons contribute to the decoding accuracy, we conducted identical analysis dividing to the stimulus preferring and non-preferring populations. Both population types showed evolving improvement as similar to whole population (Fig.3c), and the concatenated population of V1 and PPC was informative than the stimulus non-preferring populations, but equal to the stimulus preferring population in PPC. Although the above decoding analysis was applied to the neurons which are recorded in different sessions (pseudo-population), we confirmed that the population activity can predict the choice types from the population that was taken from the same sessions (ranged 5 – 21 neurons, 35 sessions, real-population). Classification accuracy was improved in real dataset compared to shuffle labeling dataset in both V1 and PPC (Fig.3d, $p < 0.05$ paired t-test), indicating the presence of population coding regardless of real- and pseudo-populations.

V1 Noise correlation was reduced in the self-initiated detection performance before and after the stimulus presentation

To further reveal the important of the population-level coding for the task performance, we investigated the impact of noise correlation on the choice types between pairs of simultaneously recorded neurons in V1 and PPC. If the noise is closer to random across neurons (low noise correlation), information coding is more reliable and efficient[64–66]. We found that noise correlation in Hit trials reduced in -0.2s – 0.2s from the stimulus onset compared to the other choice types in the V1 neuron pairs, while the PPC neuron pairs were de-correlated only in the pre-stimulus epoch (Fig.4a,b). To investigate coupling across the different cortical areas, we also analyzed neuron pairs between V1 and PPC and found that near-zero correlation was observed in Hit trials in -0.4 – 0.2s. However, the noise correlation between Miss+ and Miss- was not significantly changed in all the timings and neuron pairs. These results suggest that efficient coupling of neurons have significant impact on optimal choice behavior. We next investigated impact of other task variables on noise correlation (Fig.4c). We found that noise correlation in V1 was significantly reduced in previous peripheral reward trials after the stimulus presentation, while the previous central reward did not show such effect. Such a reduction of the noise correlation after the rewarded trials was not observed in PPC but rather it showed an unexpected increase during the pre-stimulus epoch. These results suggest that neuronal coupling in V1 plays an important role in the accurate visual detection performance, and that the reward history is partially responsible for modulating coordination of neurons for the subsequent trials.

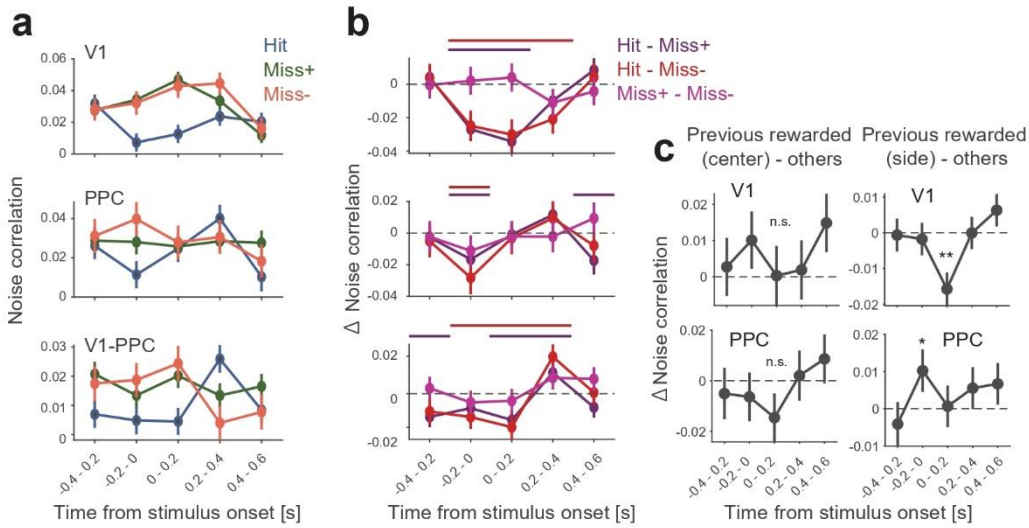

Figure 4 | Noise correlation was reduced preceding stimulus presentation. **a**, Mean noise correlations in each 200ms window in V1, PPC and V1-PPC pairs of neurons was shown as Mean ± SEM. **b**, Mean differences of noise correlation between pairs of choice types calculated from **a**. Colored bars at top indicate time points with significant non-zero differences ($p < 0.05$, Wilcoxon signed-rank test). **c**, Mean differences of noise correlation between previous rewarded and non-rewarded.

Discussion

It is widely believed that trial-by-trial variance of visual detection is attributed to fidelity of visual responses in sensory neurons. Our results rather demonstrated that the major contribution of non-sensory neurons in V1 and PPC for reliable visual detection performance. The near-threshold stimuli used in our task induced trial-by-trial variability in the visual detection performance and we further classified them into the three types of the trials with distinct perceptual states, which were not differentiated in most of the previous studies [47,57]. We showed multiple evidences for population-level coding for those choice types in V1 and PPC. First, despite no clear differences in the averaged activities among the choice types, we found specific divergence among the choice types at the level of population activity, in particular, the robust contribution of the stimulus non-preferring neurons in both V1 and PPC (Fig.2). Second, during the pre-stimulus and stimulus epochs, contributions of the individual neurons for distinct population dynamics were nearly random, indicating that neural ensembles dynamically altered to neural computation dedicated to each epoch. Third, we found that the individual neurons that poorly represented the choice types also contributed to the population coding of the choice types (Fig.3). Finally, V1 neuron pairs, but not PPC, showed near-zero noise correlation in Hit trials

prior to and during the visual stimulus presentation (Fig.4), indicating that the V1 population gains efficiency of information processing for the future behavioral output.

It has been postulated that stochastic behavioral responses to identical sensory stimuli is generated by fluctuations of background neural ensembles preceding to the external inputs [67]. Our results agree with this hypothesis in the sense that the choice types are already separable in the pre-stimulus epoch in both V1 and PPC populations. However, our results also indicate the significant role of the V1 non-sensory neurons after the stimulus presentation in segregating the choice types, suggesting distinct population-level mechanism from the pre-stimulus background fluctuations in V1. These non-sensory activities are not likely to involve in gain modulation of visual inputs (e.g., [68]), because there are no clear differences in the visual responses between the Hit and Miss+ conditions in V1 as well as PPC. Rather, we suggest that V1 non-sensory activities are necessary components for building relevant behavioral outputs. In contrast, PPC population activity showed slower decays and was spread to other epochs (Fig.2), which is in line with a previous study [69]. It is also interesting that a previous study revealed that sustain activity in parietal-frontal cortex showed stronger sustained activity when the monkey subjects consciously report the visual stimuli [4]. Our results match with their result since the sustained activity in our study also associated with Hit trials, which possibly involves in coherent representations of the choice information at population level [70].

It has been controversial whether task engagement reduce the noise correlation specifically in the area relevant to the task. Our results add an evidence that reduced noise correlation in Hit trials was specific to V1 but not PPC. Correlated noise in sensory areas is considered to filter sensory inputs from noisy environment[64,66]. However, the visual responsive neurons in V1 were less informative to segregate the choice types than the non-sensory neurons. In addition, the stimulus preferring population in PPC shows greater classification performance compared to V1 (Fig.3c), while it achieved the same level of decoding performance compared to the whole population in V1 (Fig.3b-c). Therefore, it is likely that sensory and non-sensory information is converged in PPC by feedforward projections.

Relatively weak contribution of the visually-evoked activities in V1 population coding could be an unique feature of our task design because the animals have a third option, of which experienced reward value may suppress peripheral choices even when the animals recognize the stimuli. However, ignoring the presence of stimuli is never rewarded in our task and thus highly suboptimal. In addition, our data shows that the rewards in the previous trials only partially explain the behavioral variance in Hit/Miss choices (Fig.1h) as well as the variance in noise-

correlation (Fig.4c). Therefore, we conclude that recruitments of non-sensory neurons in V1 is not due to the dominated value-based decisions. On the other hand, it is possible that irreverent movements during the task performance could have affected Hit responses due to suboptimal head/body positions [71–74]. However, our data shows the noise-correlation in V1 is specifically reduced in Hit trials, suggesting that, at least, the accurate performance in Hit trials is due to intrinsic population-level mechanism related to sensory-motor transformation during the task [57]. Although it has been indicated the significant contributions of non-sensory neurons for perceptual decision makings[42–44], most of them employs sensory categorization tasks in forced choice paradigm, which unavoidably suffers from stimulus uncertainty causing subjective biases due to value-based decisions. Our data support and extend these findings by showing that even in the simplest sensory detection task, which does not have inherent stimulus uncertainty and is less contaminated by value-based decisions, non-sensory neurons in V1 plays significant role in sensory decisions at a population level.

Acknowledgments

We would like to thank members of the Laboratory of Neural Information at Doshisha University for helpful discussion, and Yuta Tanisumi, Kazuki Shiotani, Susumu Takahashi for powerful comments. This research was supported by the JSPS KAKENHI Grant Numbers 19J21544 (to Y.O.), 20H00109, 20H05020 (to Y.S.), 19J12634 (to T.O) and 16K18380, 19H05028, 19K06948 (to J.H.).

Author Contributions

Y.O., T.O., and J.H. designed the experiments. Y.O. performed the experiments and analyzed the data. T.O. analyzed the data. H.M, Y.S. and J.H. supervised the project. All authors contributed to writing the manuscript.

Declaration of Interests

The authors declare no competing interests.

Figure Legends

Figure 1 | Neural recording in V1 and PPC during spatial visual-cue detection task. a, Schematics of behavioral paradigm. Trial was initiated by nose-poking into central port, rats earned water reward by choosing peripheral port when visual cue was presented, or by holding

nose-poking into central port when cue was not emitted. In 3C trials, central port was available, but it was shut when they kept nose-poking into central port over 0.5s. **b**, Spatial choice accuracy in 3C and FC trials with graded visual contrast in session A and one contrast in session B. **c**, Miss rate in 3C trials. **d**, Correct rejection rate in 3C trials. **e**, Spatial choice accuracy before and after shutter closure in FC trials. **f**, Conceptual illustrating of three distinct choice types. We classified spontaneous correct response, forced correct response and forced error choice as Hit, Miss+ and Miss-, respectively. **g-h**, The impact of task parameters on behavioral variability using GLM fitting. We fitted a GLM to several measures of task parameter to Left/Right choice in 3C and FC (**g**), and to Hit/Miss choice in left and right stimulus (**h**). **i**, Histogram of contralateral stimulus selectivity for V1 and PPC. Colors indicate neurons with significant selectivity. Inset indicates proportion of neurons with significant selectivity. **j**, Decoding accuracy of contralateral stimulus presence for the stimulus preferring, non-preferring population and individual sessions. Decoding in the stimulus preferring population was significantly higher compared to chance level ($p < 0.001$, one-tailed test), but there was no difference between Hit and Miss ($p > 0.05$, Methods). In the stimulus non-preferring population, there was no difference between conditions and chance level. In individual sessions (n = ### sessions), both Hit and Miss population activity was decodable compared to chance level ($p < 0.001$, t-test), and there is no difference of decoding accuracy between conditions ($p > 0.05$, t-test). **k**, Trial-averaged neural activity of Enhanced type and Suppressed type in the stimulus preferring neurons in V1 and PPC. All responses were normalized by absolute peak subtracted mean response. Neurons sorted by max peak latency in hit trials.

Figure 2 | Population dynamics in pre-stimulus and stimulus subspaces in V1 and PPC. a, b, Population responses of whole population projected onto three dimensions of the stimulus subspace from stimulus onset to stimulus offset (0-0.2s from stimulus onset) in V1 and PPC. Each color corresponds to choice types. **c, d**, Euclidian distance between pairs of conditions in PC subspace calculated from projections of **a**, **b**. Shaded area indicated stimulus presentation timing. Each plot was shown as Mean ± S.E and dashed line denotes 95% confidence interval of the shuffled distribution with 1000 shuffles. **e, f**, Same as in **c**, **d**, but calculated from the stimulus preferring and non-preferring population in V1 and PPC. **g, j**, Same as in **c**, **d**, but calculated from whole population which projected n-dimensions of the pre-stimulus subspaces (-0.2 – 0s from stimulus onset) in V1 and PPC. **h, k**, Percentages of stimulus subspace data variance (blue) and pre-stimulus data variance (red) for each epoch. **i, l**, Sum of variance explained from 10 PCs for each subspace. Histogram shows shuffled distributions with 1000 shuffles. Each significance marks were compared to shuffle data ($p < 0.001$, one-tailed test).

Figure 3 | Distributed representation by sequential population size. a, Histogram of decoding accuracy for choice types for individual neurons (colored line) and shuffled data (gray line) based on the normalized firing rate in stimulus presentation epoch (0-0.2s from stimulus onset) in V1 and PPC. **b**, Classification accuracy for choice types by sequential population size. Neurons we included by descending order based on histogram in **a** in whole population. Each line was shown as Mean ± 95% confidence interval. **c**, Same as in b, but only the stimulus preferring (left) and non-preferring neurons (right) were used. **d**, Classification accuracy for choice types in individual sessions (n = 35sessions). Real data showed significantly higher accuracy compared to shuffled data ($p < 0.05$, student t-test).

Figure 4 | Noise correlation was reduced preceding stimulus presentation. a, Mean noise correlations in each 200ms window in V1, PPC and V1-PPC pairs of neurons was shown as Mean ± SEM. **b**, Mean differences of noise correlation between pairs of choice types calculated from **a**. Colored bars at top indicate time points with significant non-zero differences ($p < 0.05$, Wilcoxon signed-rank test). **c**, Mean differences of noise correlation between previous rewarded and non-rewarded.

Methods

Subjects

Seven male Long-Evans rats (Shimizu Laboratory Supplies, Kyoto, Japan) weighting 200-268 g at the beginning of the training were individually housed and maintained on a laboratory light/dark cycle (lights on 8:00 A.M. to 9:00 P.M.). Rats were placed on water restriction with *ad libitum* access to food. The animals were maintained at 80% of their baseline weight throughout the experiments. All experiments were implemented in accordance with the guidelines for the care and use of laboratory animals provided by the Animal Research Committee of the Doshisha University.

Behavioral apparatus

The behavioral apparatus (Fig.1a) has been previously described[2]. An operant chamber (O'Hara, Tokyo, Japan) with three ports in the front wall for nose-poke responses was enclosed in a soundproof box (Brain Science Idea, Osaka, Japan). Each port was equipped with an infrared sensor to detect the animals' nose-poke responses. Visual cues were presented using white light-emitting diodes (LEDs) (4000 mcd; RS Components, Yokohama, Japan) placed on the left and right walls of the operant chamber, as in Fig.1a. Water rewards were delivered from gravity-fed reservoirs regulated by solenoid valves (The Lee Company, Westbrook, CT) through stainless

tubes placed inside of the left and right target-ports. We controlled stimulus and reward deliveries and measured behavioral responses using Bpod and Pulse Pal[75] (Sanworks, Stony Brook, NY).

Visual cue detection task

The visual cue detection task design was described previously[2]. The task was comprised of randomly interleaved three choice (3C) and forced-choice (FC) trials with equal probabilities in a session. The only difference between the trial types was that, in FC trials, the central port was shut with the shutter door to prevent the rat from continuing to central nose poke (Fig. 1a). After a fixed 2.5 s inter-trial interval (ITI), the central port was illuminated by an interior LED of the central port signaling the ready state of a trial initiation. The rats initiated each trial by making nose pokes into the central port. After a 0.2–0.6 s random stimulus delay, the visual stimulus was presented from the left or right side for a duration of 0.2 s. Rats were allowed to make a choice response after the end of the stimulus delay period. The trials where animals prematurely left the port before stimulus delay were canceled and they needed to re-initiate the trials. We randomly provided one of three levels of visual brightness (difficult, medium, and easy) for each trial by modulating the voltage ranging 0.02–5.1 lx in session A. Difficult and easy stimuli were selected for all subject based on the minimum and maximum LED voltage dynamic range. Medium stimuli were selected for each subject such that the subject detected stimuli with medium accuracy between easy and difficult stimuli in the forced-choice (FC) trials. The probabilities for left, right, or no visual stim- ulus were equal (33% per condition) in 3C and FC trials. The reward was given if rats chose the same side where the visual stimuli was emitted in the 3C and FC trials. If animals kept nose poke more than X s in the central port after the presentation of the visual stimuli, the trial was treated as miss error. X were drawn from the uniform distribution with a range of [0.5, 1]. Note that X is aligned with the expected timing of the reward delivery in no-signal trials so that animals cannot utilize the absence of reward delivery as indication of the presence of unnoticed visual stimuli. Failure of the peripheral choices within 5 s after nose withdrawal from the central port was also treated as miss error, though it occurred rarely (<5%). There was no punishment in any error trials and next trial was allowed to be initiated after ITI. In the no-signal trials, animals need to wait for 0.2–0.6 s without stimulus and another 0.5–1 s to get reward from the central port. There was no cue to distinguish the initial delay (0.2–0.6 s) and reward delay (0.5–1 s). Thus, animals did not have any external clue to differentiate the signal trials from the no-signal trials, except for the presentation of the signal itself. In the FC trials, the shutter was closed 0.5 s after stimulus presentation onset, and the rats were forced to choose either the left or right port (Fig.1a right). In cases where no stimuli were presented in FC trials, the animals were never rewarded.

Session B was same protocol with session A described above except that only single stimulus difficulty was used. To prevent contamination of Miss+ and Miss- as possible in session B, we applied stimulus contrast level of 70-85% accuracy in FC trials in session A.

Surgery

Rats were anesthetized with 2.5% isoflurane before surgery, and it was maintained throughout surgical procedures. We monitored body movements and hind leg reflex and adjusted the depth of the anesthesia as needed. An eye ointment was used to keep the eyes moistened throughout the surgery. Subcutaneous scalp injection of a lidocaine 1% solution provided local anesthesia before the incision. A craniotomy was performed over the anterior part of the right V1 (AP -6.36 to -7.32 mm, ML 3.2 mm relative to the bregma, 0.2 to 0.4 mm below the brain surface) and right PPC (AP -3.8 mm, ML 2.5 mm relative to the bregma, 0.2 to 0.4 mm below the brain surface) and a custom-designed electrode was vertically implanted using a stereotactic manipulator. A stainless-steel screw was placed over the cerebellum and served as the ground during the recordings. We used the mean response of the all electrodes as a reference. During a week of postsurgical recovery, we gradually lowered the tetrodes to detect unit activities in the V1 and PPC. Electrode placement was estimated based on the depth and was histologically confirmed at the end of the experiments.

Histology

Once the experiments were completed, the rats were deeply anesthetized with sodium pentobarbital and then transcardially perfused with phosphate-buffered saline and 4% paraformaldehyde. The brains were removed and post-fixed in 4% paraformaldehyde, and 100 µm coronal sections of the brains were prepared to confirm the recording sites.

Electrophysiological recordings

A custom-designed electrode composed of two eight-tetrodes (tungsten wire, 12.5 µm, California Fine Wire, Grover Beach, CA) was used for the extracellular simultaneous recordings of V1 and PPC. The tetrodes were individually covered by a polyimide tube (A-M Systems, Sequim, WA), were placed at a 100 µm separation and typically had an impedance of 120–1000 kΩ at 1 kHz. The signals were recorded with Open Ephys (Cambridge, MA) at a sampling rate of 30 kHz and bandpass filtered between 0.3 and 6 kHz. The tetrodes were lowered approximately 20µm after each recording session, and thereby independent populations of neurons were recorded across the sessions.

Spike sorting and screening criteria of units

All analyses were performed using MATLAB (MathWorks, Natick, MA). To detect single-neuron responses, the spikes were manually clustered with MClust (A.D. Redish) for MATLAB. Only neurons met the following criteria were included for further analyses: (1) units with sufficient isolation quality (isolation distance ≧ 15); (2) units with reliable refractory periods (violations were less than 1% of all spikes); and (3) units with sufficient mean firing rates in the 1 s after the cue onset (> 1 Hz). On average,

Behavioral data analysis

Spatial choice accuracy was the percentage of peripheral port choices where visual stimuli were presented, regardless of the correctness of the choice side (Fig.1b). The miss rate was the percentage of central port choices in trials where visual stimuli were presented in 3C trials (Fig.1c). The correct rejection rate was the percentage of central choices in trials where visual stimuli were not emitted in 3C trials (Fig.1d). Reaction time was defined as the duration from stimulus presentation onset to nose withdrawal from the central hole. Trials with a reaction time of less than 100 ms was considered as invalid, and were excluded from the calculation of the spatial choice accuracy as they were too early to have been responses to the stimulus[76]. All error bar data are presented as mean ± SEM. In all violin plots, it combined a boxplot with the kernel density estimation procedure. The boxplot inside the violin showed the quartile, whisker and median values as white dots (Extended Data Fig.2a-h).

We classified following three choice types based on the subjects' detection performance (Fig.1f): (1) Hit was the trials where subject performed peripheral choice in 3C or spatial choice before shutter closure in FC. (2) Miss+ was the trials where they nose-poked in central port over 0.5s and they could choose correct peripheral choice in forced choice by shutter closure. (3) Miss- was error choice in forced choice. Trials with miss response in 3C were excluded from the analysis of comparison across choice types because we cannot label the trials into Miss+ or Miss-.

To estimate the impact of task parameters on behavioral performance, we conducted generalized linear model (GLM) analysis for spatial choice (Left/Right) and hit/miss choice (Fig.1g-h). Due to behavioral performance in 3C trials for spatial choice was near perfect (90% choice accuracy), we used identity function as link function. In other model, we used logit function as link function. For spatial choice GLM analysis, we prepared trials which they performed peripheral choice. Task parameters included with binary predictors of stimulus (1 was stimulus presence, and 0 otherwise), peripheral previous reward (1 was rewarded, 0 otherwise), and central previous reward (1 was rewarded, 0 otherwise). Model was fit with these predictors. For hit/miss choice GLM analysis, we first prepared trials which stimulus is presence. Task parameters included with binary predictors of peripheral previous reward (1 was

rewarded, 0 otherwise), central previous reward (1 was rewarded, 0 otherwise) and previous failure (1 was failed, 0 otherwise). Then we fitted model to behavioral performance as same procedure as spatial choice GLM analysis.

Selective responses to visual stimulus

Neurons were classified as the visual stimulus preferring neurons or non-stimulus preferring neurons based on their mean response during visual stimulus presentation (0.2s window from stimulus onset) (Fig.1i). Modulation index was computed using a receiver operating characteristic (ROC) analysis, which is to provide a measure of the difference of neural firing distribution between trial types based on single trial response[63]. We compared distribution between the trials in visual stimulus presence and absence. The visual stimulus selectivity was obtained from the area under ROC curve (AUC) and defined as $2 \times (\mathrm{AUC}-0.5)$ ranging from -1 to 1. In our analysis, a positive value indicated a neuron selectively fired to the visual stimulus (Enhanced type), and a negative value indicated to suppress (Suppressed type). A value of zero indicated the absence of visual stimulus selective responses. To determine statistical significance ($P < 0.05$), we used permutation tests (2,000 iteration).

Spike train analysis

We recorded 966 neurons (V1: 518, PPC: 448 neurons) from 62 sessions in seven rats. Unless otherwise stated, the activity of each neuron was binned at 0.005s, smoothed with a causal Gaussian filter with standard deviation 0.025s to obtain the temporal profile of each neural activity.

For visualization (Fig.1k), we averaged firing rate across trials in the analysis window (-0.5 – 1.0s from stimulus onset), subtracted baseline activity (-0.2 – 0s from stimulus onset) and normalized by dividing by absolute max firing rate ranging from -1 to 1.

Statistics

We evaluated the statistical significance of the state space analysis with a bootstrapping procedure (ref). We estimated the P value for the bootstrapping procedure by computing the ratio $(1+X) / (N+1)$, where the number X indicates overlapping data points between the two distributions and the number N indicates iterations. Since we used 1,000 bootstraps, two distributions with no overlap resulted in $P < 0.001$, and two distributions with x% overlap resulted in $P \approx x/100$.

State space analysis

Before application of principal component analysis (PCA), we extracted neurons which recoded at least 10 trials of each condition. To characterize population structure and temporal pattern between all neurons during stimulus epoch, normalized firing rates were formatted as $X^{stim} \in \mathbb{R}^{N \times CT}$, where N is the total number of neurons, C is the total number of conditions and T is the number of analyzed time points. In a same fashion, we constructed matrix during pre-stimulus epoch as $X^{pre-stim} \in \mathbb{R}^{N \times CT}$. Here, PCA is used to parameterize key difference across conditions in each epoch and reduced dimensionality of population from number of neurons to three principal components (PCs). Each PC represents weighted combination of individual neural activity, which summarized population activity.

To estimate the difference of each neural trajectories at each time points with respect to choice types, we computed the signed Euclidian distance between pairs of conditions in the PCs spaces, of which dimensions were used to reach above 70% variance explained. This procedure was repeated 1000 times with different subsets of ten trials for each choice type (Fig.2c). To estimate the statistical difference, we computed distance of shuffled data as same procedures described above, which is constructed by shuffled PC weights to neural data.

Classification (decoding) analysis

For classifiers, we mainly used a support vector machines (SVM) with a linear kernel implemented using the MATLAB functions. All population classification was analyzed on the concatenated normalized activity of individual neurons. Because most of our neurons were not simultaneous recoded, we constructed 'pseudo-trials' by randomly extracting trials from desired conditions for each neuron. Data were divided into non-overlapped training/validation and test data (15% trials). To avoid overfitting, models were trained exclusively on the train/validation data set. Hyperparameters such as C and Υ; regularization weight and radial basis function width, respectively, was determined by optimization to minimize loss of 10-fold cross-validation.

For two-class classification such as classification of stimulus (presence/absence) (Fig.1j), we used normalized firing rate in stimulus epoch (0 – 0.2s from stimulus onset) for each individual neuron. We then concatenated neural activity as described above and performed training and predictions. For three-class classification such as classification of choice types (Hit/Miss+/Miss-) (Fig.3a), we used normalized firing rate in pre-stimulus and stimulus epoch (-0.2 – 0s and 0 – 0.2s from stimulus onset, respectively). In this analysis, we constructed error correcting output code (ECOC) model which is multi classification model with combined binary SVM model for multi-class decoding.

For classification by adding-in subsets of neurons (Fig.3b, c), classifier (SVM model) was built by same procedure described above in each subpopulation. This subpopulation was divided into 20 equal proportion. Each 20 group was constructed in ascending order of classification accuracy of individual neurons.

For classification of simultaneous recoding population (Fig.3d), we first extracted sessions which contains at least five neurons in each region (35 sessions) and contained at least seven trials in each condition. Therefore, we trained classifier as similar procedure described above and predicted the test data.

Noise correlation

In this study, noise was defined as trial-by-trial variability of mean subtracted firing rate. Noise correlation was defined as the correlation coefficients between the noise of neuron pairs to a given visual stimulus. For calculation of noise correlation, we computed z-scored firing rate for a given visual stimulus, allowing us to evaluate correlations between noises with subtraction of response correlation. We applied this analysis to spike counts from a 200ms window during -0.4 – 0.6s from stimulus onset (Fig.4). In this analysis, we selected neurons with at least ten trials with respect to condition. For statistical significance of noise correlation between conditions, we computed difference of noise correlation (Δ noise correlation) between pairs of possible different conditions, and Wilcoxon signed-rank test was performed in each time window (Fig.4b-c).

Extended data

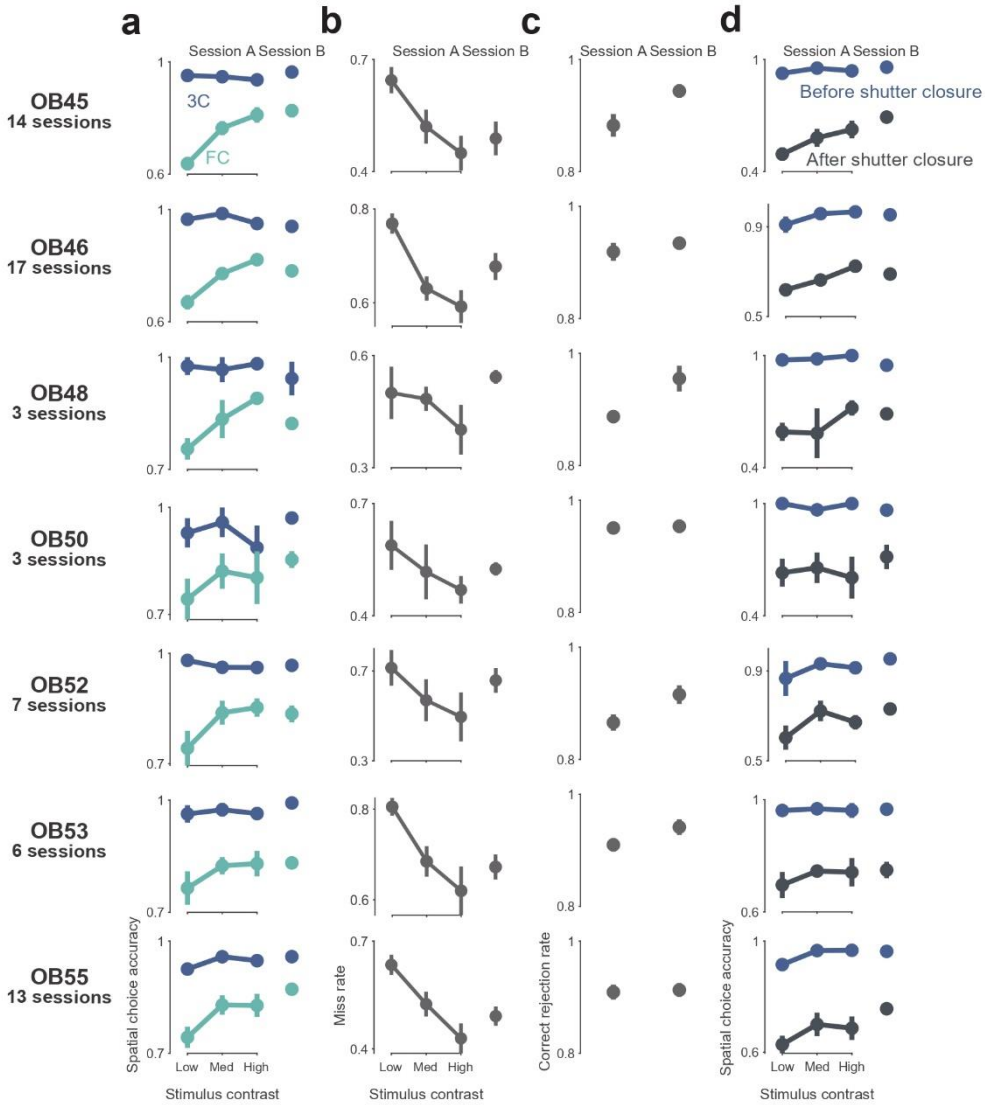

Extended Data Fig 1 | Behavioral performance in visual detection task for each subject. a, Spatial choice accuracy in 3-choice (3C) and forced-choice (FC) trials for each subject. The vertical axis indicates accuracy and horizontal axis indicates three graded stimulus contrast in session A and one contrast in session B. Each subject showed above 90% accuracy in 3C trials and graded accuracy with stimulus contrast in FC trials **b**, Miss rate in 3C trials for each subject in session A and B. Each subject showed decrease of miss rate with increase of stimulus contrast. **c**, Correct rejection rate for each subject in session A and B. Each subject showed about 90% accuracy in both session A and B. **d**, Spatial choice accuracy in FC trials for each

subject in session A and B. Colors correspond to choice timing (blue: before shutter closure, black: after shutter closure).

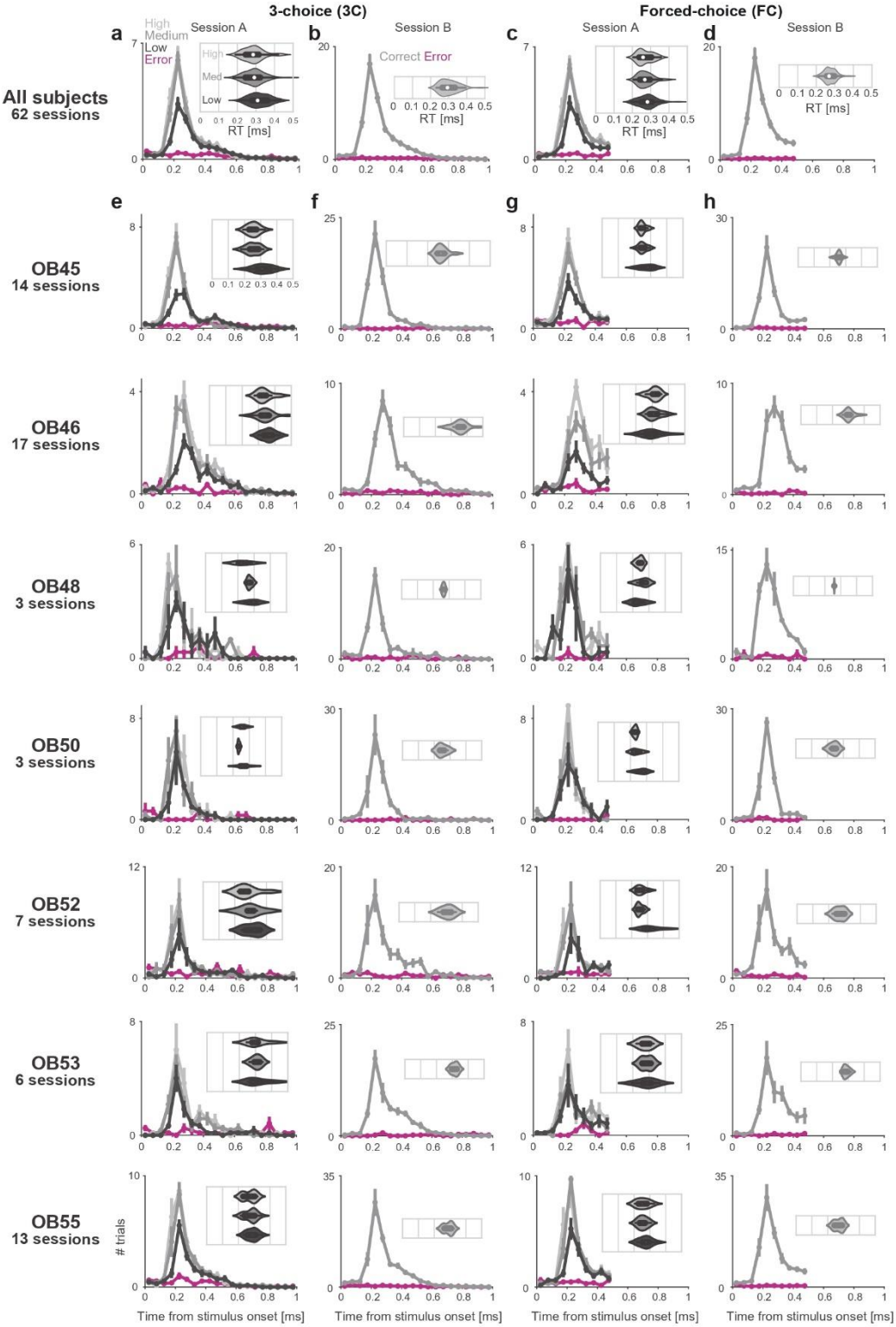

Extended Data Fig 2 | Reaction time in each subject. a, Distribution of reaction timing in 3C trials of all subjects in session A. Colors correspond visual contrast and error. Inset shows violin plots of reaction timing in each stimulus contrast. White circles indicate median value and end of thick line indicates quartiles. **b,** Same as in **a**, but in session B. **c,** Same as in **a**, but in FC trials. Because of shutter closure, reaction timing was not defined after 0.5s from stimulus onset. **d,** Same as in **b**, but in session B. **e-h,** Same as in **a-d** for each subject.

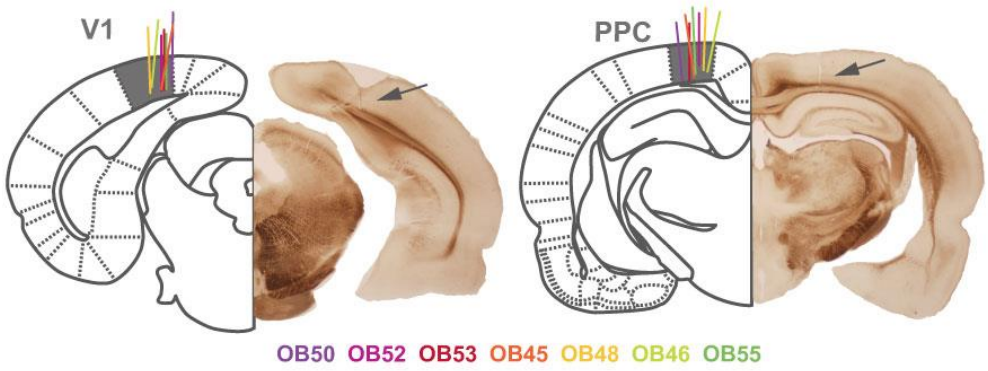

Extended Data Fig 3 | Recoding sites in V1 and PPC. Coronal section indicating recoding sites in V1 and PPC (arrow). We recoded neural activity in V1 and PPC simultaneously from seven rats. Each color corresponds to subject ID.

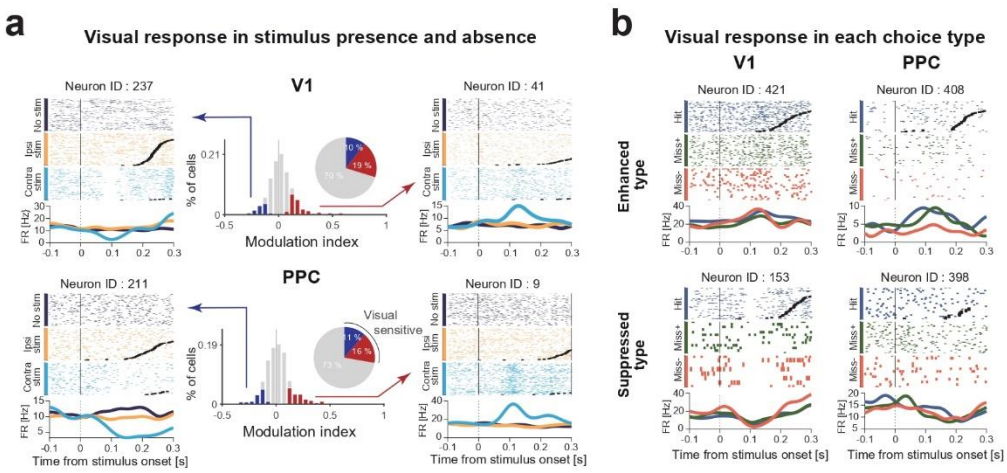

Extended Data Fig 4 | Neural response properties in the stimulus preferring neurons. a, Visual responses of example stimulus preferring neurons in V1 and PPC. Histograms indicate proportion of modulation index in V1 and PPC (same figure in Fig.1i). Colors indicate

significant modulation index compared to shuffled data ($p < 0.05$, permutation test). Raster sorted by No-stimulus, ipsi-stimulus and contra-stimulus, and trial-averaged firing rates (smoothed with 25ms gaussian filter) for each stimulus condition. Black dots in raster plot indicate reaction timing. **b,** Raters sorted by choice types, and trial-averaged firing rates for Enhanced and Suppressed types in V1 and PPC. Black dots in raster plot indicate reaction timing.

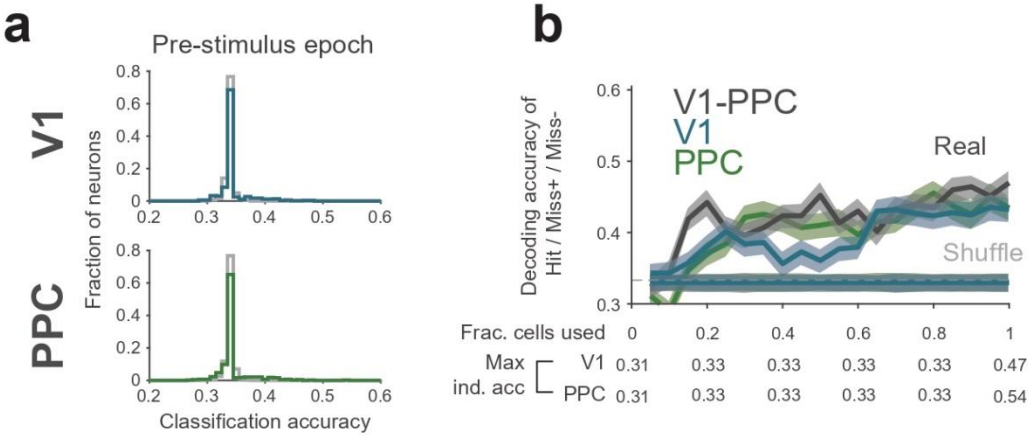

Extended Data Fig 5 | Distributed representation by sequential population size in pre-stimulus epoch. a, Histogram of classification accuracy for choice types for individual neurons (colored line) and shuffled data (gray line) based on the normalized firing rates in pre-stimulus epoch (-0.2 – 0s from stimulus onset). **b,** Classification accuracy for choice types by sequential population size. Each line was shown as mean ± 95% confidence interval.

References

1. Foote, A. L. & Crystal, J. D. Metacognition in the Rat. *Curr. Biol.* **17**, 551–555 (2007).
2. Osako, Y., Sakurai, Y. & Hirokawa, J. Subjective decision threshold for accurate visual detection performance in rats. *Sci. Rep.* **8**, 1–10 (2018).
3. Rabbitt, P. M. Errors and error correction in choice-response tasks. *J. Exp. Psychol.* **71**, 264–272 (1966).
4. Bram van, V. *et al.* The threshold for conscious report: Signal loss and response bias in visual and frontal cortex. *Science (80-.).* **7186**, (2018).

5. Peters, M. A. K. & Lau, H. Human observers have optimal introspective access to perceptual processes even for visually masked stimuli. *Elife* **4**, 1–30 (2015).
6. Merikle, P. M., Smilek, D. & Eastwood, J. D. Perception without awareness: Perspectives from cognitive psychology. *Cognition* **79**, 115–134 (2001).
7. Kolb, F. C. & Braun, J. Blindsight in normal observers. *Nature* **377**, 336–338 (1995).
8. Snodgrass, M. & Shevrin, H. Unconscious inhibition and facilitation at the objective detection threshold: Replicable and qualitatively different unconscious perceptual effects. *Cognition* **101**, 43–79 (2006).
9. Osborne, L. C., Hohl, S. S., Bialek, W. & Lisberger, S. G. Time course of precision in smooth-pursuit eye movements of monkeys. *J. Neurosci.* **27**, 2987–2998 (2007).
10. Parker, A. J. & Newsome, W. T. SENSE AND THE SINGLE NEURON: Probing the Physiology of Perception. *Annu. Rev. Neurosci.* **21**, 227–277 (1998).
11. Shadlen, M. N. & Newsome, W. T. The variable discharge of cortical neurons: implications for connectivity, computation, and information coding. *J. Neurosci.* **18**, 3870–3896 (1998).
12. Tolhurst, D. J., Movshon, J. A. & Dean, A. F. The statistical reliability of signals in single neurons in cat and monkey visual cortex. *Vision Res.* **23**, 775–785 (1983).
13. Tomko, G. J. & Crapper, D. R. Neuronal variability: non-stationary responses to identical visual stimuli. *Brain Res.* **79**, 405–418 (1974).
14. WERNER, G. & MOUNTCASTLE, V. B. the Variability of Central Neural Activity in a Sensory System, and Its Implications for the Central Reflection of Sensory Events. *J. Neurophysiol.* **26**, 958–977 (1963).
15. Busse, L. *et al.* The detection of visual contrast in the behaving mouse. *J. Neurosci.* **31**, 11351–11361 (2011).
16. Bagur, S. *et al.* Go/No-Go task engagement enhances population representation of target stimuli in primary auditory cortex. *Nat. Commun.* **9**, (2018).
17. Smallwood, J. & Schooler, J. W. The restless mind. *Psychol. Bull.* **132**, 946–958 (2006).
18. Aston-Jones, G. & Cohen, J. D. An Integrative Theory of Locus Coeruleus-Norepinephrine Function: Adaptive Gain and Optimal Performance. *Annu. Rev. Neurosci.* **28**, 403–450 (2005).
19. Musall, S., Urai, A. E., Sussillo, D. & Churchland, A. K. Harnessing behavioral diversity to understand neural computations for cognition. *Curr. Opin. Neurobiol.* **58**, 229–238 (2019).
20. Critchley, H. D. & Rolls, E. T. Hunger and satiety modify the responses of olfactory and visual neurons in the primate orbitofrontal cortex. *J. Neurophysiol.* **75**, 1673–1686 (1996).

21. Schriver, B. J., Bagdasarov, S. & Wang, Q. Pupil-linked arousal modulates behavior in rats performing a whisker deflection direction discrimination task. *J. Neurophysiol.* **120**, 1655–1670 (2018).
22. Harris, K. D. & Thiele, A. Cortical state and attention. *Nat. Rev. Neurosci.* **12**, 509–523 (2011).
23. Monto, S., Palva, S., Voipio, J. & Palva, J. M. Very slow EEG fluctuations predict the dynamics of stimulus detection and oscillation amplitudes in humans. *J. Neurosci.* **28**, 8268–8272 (2008).
24. Gilden, D. L. Cognitive emissions of 1/f noise. *Psychol. Rev.* **108**, 33–56 (2001).
25. Niell, C. M. & Stryker, M. P. Modulation of Visual Responses by Behavioral State in Mouse Visual Cortex. *Neuron* **65**, 472–479 (2010).
26. McGinley, M. J. *et al.* Waking State: Rapid Variations Modulate Neural and Behavioral Responses. *Neuron* **87**, 1143–1161 (2015).
27. McCormick, D. A., McGinley, M. J. & Salkoff, D. B. Brain state dependent activity in the cortex and thalamus. *Curr. Opin. Neurobiol.* **31**, 133–140 (2015).
28. Lee, S. H. & Dan, Y. Neuromodulation of Brain States. *Neuron* **76**, 209–222 (2012).
29. Jacobs, E. A. K., Steinmetz, N. A., Carandini, M., Harris, K. D. & Uk, K. Cortical state fluctuations during sensory decision making. *bioRxiv* 1–22 (2017) doi:10.1101/348193.
30. Shimaoka, D., Steinmetz, N. A., Harris, K. D. & Carandini, M. The impact of bilateral ongoing activity on evoked responses in mouse cortex. *Elife* **8**, 1–19 (2019).
31. Lak, A. *et al.* Dopaminergic and Prefrontal Basis of Learning from Sensory Confidence and Reward Value. *Neuron* **105**, 700-711.e6 (2020).
32. Lak, A., Nomoto, K., Keramati, M., Sakagami, M. & Kepecs, A. Midbrain Dopamine Neurons Signal Belief in Choice Accuracy during a Perceptual Decision. *Curr. Biol.* **27**, 821–832 (2017).
33. Daw, N. D., O'Doherty, J. P., Dayan, P., Seymour, B. & Dolan, R. J. Cortical substrates for exploratory decisions in humans. *Nature* **441**, 876–879 (2006).
34. Gold, J. I., Law, C. T., Connolly, P. & Bennur, S. The relative influences of priors and sensory evidence on an oculomotor decision variable during perceptual learning. *J. Neurophysiol.* **100**, 2653–2668 (2008).
35. Akaishi, R., Umeda, K., Nagase, A. & Sakai, K. Autonomous Mechanism of Internal Choice Estimate Underlies Decision Inertia. *Neuron* **81**, 195–206 (2014).
36. Fan, Y., Gold, J. I. & Ding, L. Ongoing, rational calibration of reward-driven perceptual biases. *Elife* **7**, 1–26 (2018).
37. Fritsche, M., Mostert, P. & de Lange, F. P. Opposite Effects of Recent History on Perception and Decision. *Curr. Biol.* **27**, 590–595 (2017).

38. Hwang, E. J., Dahlen, J. E., Mukundan, M. & Komiyama, T. History-based action selection bias in posterior parietal cortex. *Nat. Commun.* **8**, 1–14 (2017).
39. Hwang, E. J. *et al.* Corticostriatal Flow of Action Selection Bias. *Neuron* **104**, 1126-1140.e6 (2019).
40. Hirokawa, J., Vaughan, A., Masset, P., Ott, T. & Kepecs, A. Frontal cortex neuron types categorically encode single decision variables. *Nature* **576**, 446–451 (2019).
41. Masset, P., Ott, T., Lak, A., Hirokawa, J. & Kepecs, A. Behavior- and modality-general representation of confidence in orbitofrontal cortex. *Cell* 1–11 (2020) doi:10.1016/j.cell.2020.05.022.
42. Safaai, H., von Heimendahl, M., Sorando, J. M., Diamond, M. E. & Maravall, M. Coordinated population activity underlying texture discrimination in rat barrel cortex. *J. Neurosci.* **33**, 5843–5855 (2013).
43. Leavitt, M. L., Pieper, F., Sachs, A. J. & Martinez-Trujillo, J. C. Correlated variability modifies working memory fidelity in primate prefrontal neuronal ensembles. *Proc. Natl. Acad. Sci. U. S. A.* **114**, E2494–E2503 (2017).
44. Insanally, M. N. *et al.* Spike-timing-dependent ensemble encoding by non-classically responsive cortical neurons. *Elife* **8**, 1–31 (2019).
45. Lamme, V. a, Supèr, H., Landman, R., Roelfsema, P. R. & Spekreijse, H. The role of primary visual cortex (V1) in visual awareness. *Vision Res.* **40**, 1507–21 (2000).
46. Silvanto, J., Muggleton, N., Lavie, N. & Walsh, V. The perceptual and functional consequences of parietal top-down modulation on the visual cortex. *Cereb. Cortex* **19**, 327–330 (2009).
47. Goard, M. J., Pho, G. N., Woodson, J. & Sur, M. Distinct roles of visual, parietal, and frontal motor cortices in memory-guided sensorimotor decisions. *Elife* **5**, 1–30 (2016).
48. Weiskrantz, L. Blindsight: a Case Study in its Implications. (1986).
49. Campion, J., Latto, R. & Smith, Y. M. Is blindsight an effect of scattered light, spared cortex, and near-threshold vision? *Behav. Brain Sci.* **6**, 423–448 (1983).
50. Glickfeld, L. L., Histed, M. H. & Maunsell, J. H. R. Mouse primary visual cortex is used to detect both orientation and contrast changes. *J. Neurosci.* **33**, 19416–22 (2013).
51. Marzi, C. A., Mancini, F. & Savazzi, S. Interhemispheric transfer of phosphenes generated by occipital versus parietal transcranial magnetic stimulation. *Exp. Brain Res.* **192**, 431–441 (2009).
52. Fried, P. J., Elkin-Frankston, S., Rushmore, R. J., Hilgetag, C. C. & Valero-Cabre, A. Characterization of visual percepts evoked by noninvasive stimulation of the human posterior parietal cortex. *PLoS One* **6**, 1–12 (2011).

53. Mazzi, C., Mancini, F. & Savazzi, S. Can IPS reach visual awareness without V1? Evidence from TMS in healthy subjects and hemianopic patients. *Neuropsychologia* **64**, 134–144 (2014).
54. Hishida, R. *et al.* Feedback inhibition derived from the posterior parietal cortex regulates the neural properties of the mouse visual cortex. *Eur. J. Neurosci.* **50**, 2970–2987 (2019).
55. Marques, T., Nguyen, J., Fioreze, G. & Petreanu, L. The functional organization of cortical feedback inputs to primary visual cortex. *Nat. Neurosci.* **21**, (2018).
56. Keller, A. J., Roth, M. M. & Scanziani, M. Feedback generates a second receptive field in neurons of the visual cortex. *Nature* 1–5 (2020) doi:10.1038/s41586-020-2319-4.
57. Pho, G. N., Goard, M. J., Woodson, J., Crawford, B. & Sur, M. Task-dependent representations of stimulus and choice in mouse parietal cortex. *Nat. Commun.* **9**, (2018).
58. Montijn, J. S., Goltstein, P. M. & Pennartz, C. M. A. Mouse V1 population correlates of visual detection rely on heterogeneity within neuronal response patterns. *Elife* **4**, 1–31 (2015).
59. Reep, R. L., Chandler, H. C., King, V. & Corwin, J. V. Rat posterior parietal cortex: topography of corticocortical and thalamic connections. *Exp. Brain Res.* **100**, 67–84 (1994).
60. Song, Y. H. *et al.* A Neural Circuit for Auditory Dominance over Visual Perception. *Neuron* **93**, 940-954.e6 (2017).
61. Wang, Q., Sporns, O. & Burkhalter, A. Network analysis of corticocortical connections reveals ventral and dorsal processing streams in mouse visual cortex. *J. Neurosci.* **32**, 4386–4399 (2012).
62. Hanks, T. D. *et al.* Distinct relationships of parietal and prefrontal cortices to evidence accumulation. *Nature* **520**, 220–223 (2015).
63. Green, D. M. & Swets, J. A. *Signal detection theory and psychophysics. (Wiley, New York, 1966)* (John Wiley, 1966).
64. Averbeck, B. B., Latham, P. E. & Pouget, A. Neural correlations, population coding and computation. *Nat. Rev. Neurosci.* **7**, 358–366 (2006).
65. Cohen, M. R. & Kohn, A. Measuring and interpreting neuronal correlations. *Nat. Neurosci.* **14**, 811–819 (2011).
66. Rumyantsev, O. I. *et al.* Fundamental bounds on the fidelity of sensory cortical coding. *Nature* **580**, 100–105 (2020).
67. Speed, A., Del Rosario, J., Burgess, C. P. & Haider, B. Cortical State Fluctuations across Layers of V1 during Visual Spatial Perception. *Cell Rep.* **26**, 2868-2874.e3 (2019).
68. Davidson, T. J. *et al.* Thalamic control of sensory selection in divided attention. *Nature* **526**, 705–709 (2015).

69. Runyan, C. A., Piasini, E., Panzeri, S. & Harvey, C. D. Distinct timescales of population coding across cortex. *Nature* **548**, 92–96 (2017).

70. Ohnuki, T., Osako, Y., Manabe, H., Sakurai, Y. & Hirokawa, J. Dynamic coordination of the perirhinal cortical neurons supports coherent representations between task epochs. *bioRxiv* 1–3 (2020).

71. Steinmetz, N. A., Zatka-Haas, P., Carandini, M. & Harris, K. D. Distributed coding of choice, action, and engagement across the mouse brain. *Nature* **in press**, 266–273 (2019).

72. Musall, S., Kaufman, M. T., Juavinett, A. L., Gluf, S. & Churchland, A. K. Single-trial neural dynamics are dominated by richly varied movements. *Nat. Neurosci.* **22**, 1677–1686 (2019).

73. Krumin, M., Lee, J. J., Harris, K. D. & Carandini, M. Decision and navigation in mouse parietal cortex. *Elife* **7**, 1–18 (2018).

74. Erlich, J. C., Bialek, M. & Brody, C. D. A cortical substrate for memory-guided orienting in the rat. *Neuron* **72**, 330–343 (2011).

75. Sanders, J. I. & Kepecs, A. A low-cost programmable pulse generator for physiology and behavior . *Frontiers in Neuroengineering* vol. 7 43 (2014).

76. Histed, M. H., Carvalho, L. A. & Maunsell, J. H. R. Psychophysical measurement of contrast sensitivity in the behaving mouse. *J. Neurophysiol.* **107**, 758–765 (2012).